Supporting Information (SI) Appendix

KDM4B protects against obesity and metabolic dysfunction

Yingduan Cheng[a,1], Quan Yuan[a,1], Laurent Vergnes[b], Xin Rong[c], Ji Youn Youn[d], Jiong Li[a], Yongxin Yu[a], Wei Liu[a], Hua Cai[d], Jiandie Lin[e], Peter Tontonoz[c], Christine Hong[f], Karen Reue[b], Cun-Yu Wang[a,g *]

[a]Laboratory of Molecular Signaling, Division of Oral Biology and Medicine, School of Dentistry, UCLA, Los Angeles, CA 90095, USA. [b]Department of Human Genetics, David Geffen School of Medicine, UCLA, Los Angeles, CA 90095, USA. [c]Department of Pathology and Laboratory Medicine, David Geffen School of Medicine, UCLA, Los Angeles, CA 90095, USA. [d]Department of Anesthesiology, David Geffen School of Medicine, UCLA, Los Angeles, CA 90095, USA. [e]Life Sciences Institute and Department of Cell & Developmental Biology, University of Michigan, Ann Arbor, MI 48109, USA. [f]Division of Growth and Development, School of Dentistry and UCLA, Los Angeles, CA 90095, USA. [a,g]Department of Bioengineering, Henry Samueli School of Engineering and Applied Science, Broad Stem Cell Research Center, and Jonsson Comprehensive Cancer Center, UCLA, Los Angeles, CA 90095, USA.

[1]Y. Cheng and Q. Yuan are the co-first authors

Materials and Methods

Histology.

Epi, SubQ, BAT, liver, and pancreatic tissues were fixed in 10% neutral-buffered formalin for 24 hours. Tissues were embedded in paraffin and sectioned at 4um. H&E staining was performed according to the standard protocols. Pancreatic islets area was presented as an average score and 6 mice per group were counted. For Oil Red O staining, liver tissue was fixed in 1% formalin for 2 hours and embedded in OCT compound. The tissue was sectioned at 10μm and stained with Oil red O according to standard methods.

Lipids and insulin measurement.

Serum triglyceride, total cholesterol, LDL cholesterol, and VLDL cholesterol lipid measurements were performed in Clinical Laboratory UCLA Division of Laboratory Animal Medicine. Free fatty acid levels were performed according to the manufacturer's protocol (Wako Diagnostics). Insulin levels were tested with an insulin kit from Biorbyt. All lipid from feces were extracted according to the protocol described before (1).

GTT and ITT.

For GTT, mice received an IP injection of glucose (2g/kg body weight) after 16 hours of fasting. Blood was collected via the tail vein at 0, 15, 30, 60, 90 and 120 minutes. The blood glucose concentration was determined by glucometer. For ITT, mice were deprived of food for 4 hours and then an IP injection of insulin (0.75 units/body weight) were administered. Blood was collected from the tail vein at 0, 15, 30, 60 and 90 minutes and blood glucose concentrations were tested.

Indirect calorimetry and oxygen consumption rate.

For indirect calorimetry, mice were individually housed for a week prior to the measurements. Indirect calorimetry was measured for 5 consecutive days. Energy expenditure was normalized by lean mass (2). The energy expenditure ANCOVA analysis done for this work was provided by the NIDDK Mouse Metabolic Phenotyping Centers (MMPC, www.mmpc.org) using their Energy Expenditure Analysis page (http://www.mmpc.org/shared/regression.aspx) Oxygen consumption rates (OCR) in fresh tissues were measured with an XF24 Analyzer (Seahorse Bioscience) as described previously (3). Freshly isolated tissues were minced and rinsed in PBS, placed in a Seahorse Islet Plate (3-5 mg per well), and incubated with 625 µl of unbuffered DMEM (containing 25 mM glucose, 1mM pyruvate, 2mM glutamine) 1 hr prior to measurements. Mixing, waiting and measurement times were 3, 2, and 3 min, respectively. OCR was measured at the baseline and after the injection of 0.75 µM FCCP.

Lipolysis.

Lipolysis analysis for cells was performed according to the manufacturer's protocol (Biovison). For the ex vivo assay, 50 mg samples of fat were put in 1.5 ml tubes containing 500 µL of Krebs Ringer Buffer (KRB, 12mM HEPES, 121 mM; NaCl, 4.9 mM KCl, 1.2 mM MgSO4, 0.33 mM CaCl2, 2% fatty-acid free BSA and 0.1% glucose (5.5 mM). Samples were minced by scissors. One sample was for the basal condition and the second sample was for the stimulated condition by 10 µM isoproterenol. An amount of 50 µl samples were collected at time points of 0 hr, 1 hr, 2 hr and 4 hr. Glycerol levels were determined by Lipolysis Colorimetric Assay Kit (Biovison). All experiments were repeated at least three times.

Cold treatment.

Mice were housed in a single cage and kept at 4^{o}C for 6 hours. Temperature was measured in conscious mice at each hour using a BAT-12 digital thermometer (Physitemp) with a Ret-3 rectal probe designed for mice. After 6 hours, fat tissues were collected for RNA extraction and ChIP assay.

RNA extraction, qRT-PCR and gene expression study.

Total RNA was extracted from the cells or tissues with Trizol reagent according to the manufacturer's protocol (Invitrogen). The cDNA was synthesized with Random hexamers by using SuperScript III (Invitrogen). qRT-PCR analysis was carried out with iQ SYBR Green Supermix (Bio-Rad) on an iCycler iQ real-time PCR detection system (Bio-Rad). 36B4 or Hprt was used as internal controls. All primer sequences were listed in Table S1. The procedure of microarray and data analysis was described before (4). In brief, One µg of RNA

from each sample was hybridized to Affymetrix Mouse 430 2.0 Arrays at the UCLA DNA Microarray Facility. Microarray cluster analysis was described before (5).

ChIP-qPCR and ChIP-Seq assays.

The chromatin immunoprecipitation protocol was described previously (6, 7). For ChIP in adipose tissue, we obtained the nuclear extract first (7). Briefly, adipose tissue was minced into small pieces using two pairs of sterile surgical scissors and fixed with 1% formaldehyde for 15 min. Cross-linking was stopped by adding glycine to a final concentration of 125mM for additional incubation with moderate shaking. Samples were then centrifuged at 2,500 rpm for 5 min, and placed on ice until the end of the procedure. Three distinct phases could be readily visualized at this point: 1) tissue aggregates of higher density (pellet, tissue debris), 2) buffer containing the PBS, formaldehyde and glycine (intermediate liquid phase), and 3) lipid-rich (low-density) tissue pieces and fat (upper layer). The upper phase was kept and washed twice with ice-cold 1× PBS supplemented with PI followed by centrifugation (2,500 rpm, 5 min, 4°C). Small adipose pieces were re-suspended in 3 ml of adipocyte lysis buffer (0.02M Tris, PH 8.0, 80 mM KCl, and 0.5% NP-40) supplemented with PI and homogenized using a Dounce homogenizer (20 strokes). Then the samples were kept on ice for 15 min to ensure rupture of the cell membranes and the release of the nuclei. Twenty additional strokes were carried out followed by a larger particle removal using 250 μm mesh. The samples were centrifuged (5 min, 2,500 rpm, 4°C) and the pellet of the nuclei was re-suspended in 500 μl of SDS lysis buffer supplemented with PI (1% SDS, 10 mM EDTA, pH 8.1, and 50 mM Tris·HCl, pH 8.1), transferred to a sterile 1.5-ml Eppendorf tube and incubated on ice for 10 min prior to sonication. A standard protocol was followed after sonication. The antibodies we used were: KDM4B (Bethyl, A301-478A), H3K9me3 (abcam, ab8898), CREB (abcam, ab31387), H4ac (Active motif, 39243), and normal Rabbit IgG (Millipore, 12-370). For ChIP-seq of Flag-KDM4B, preadiocytes were isolated from Kdm4b KO mice, Kdm4b-/-preadiocytes were infected with retroviruses expressing Flag-KDM4B or the empty vector and selected with puromycin for one week. Subsequently, cells were induced to differentiate into adipocytes that were utilized for ChIP-Seq. ChIP was performed, as described before, with Mouse Flag M2 antibody (Sigma, F3165) (8). Libraries were prepared using KAPA Hyper Prep Kit according to the manufacturer's protocol. The sequencing was performed at Clinical Microarray Core, UCLA with HiSeq 2000 system (Illumina). The analysis of ChIP-Seq data was described before (8). All sequencing reads were mapped to NCBI build 37 (mm9) of mouse genome using the software Bowtie. Here, a P value<1.0 × 10−4 was chosen to give a false discovery rate of <5%. Only reads that aligned to a unique genomic position with no more than two mismatches were retained for the above analysis. Only one read was counted if multiple reads mapped to the same position in the genome at the same time. Representative ChIP-seq enriched regions were visualized in the Integrated Genome Browser. Genes with significant peaks within 5 kb of their TSSs were considered as bound.

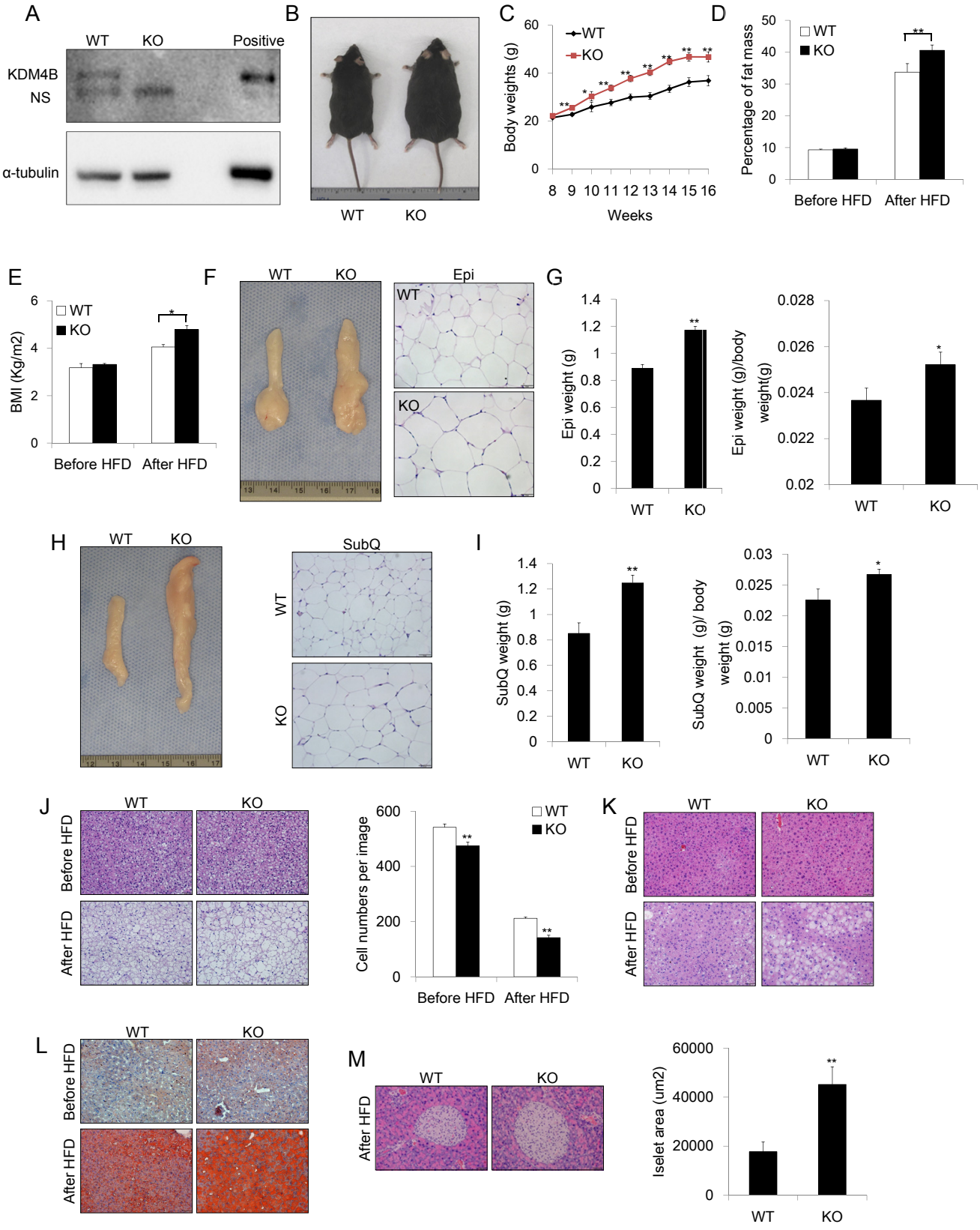

Figure. S1. Whole body *Kdm4b* knockout mice on HFD display accelerates the onset of obesity. ***(A)*** Confirming KDM4B deletion by Western blot. ***(B)*** Representative images of male 4-month-old WT and knockout (KO) mice after HFD feeding. ***(C)*** Growth curve of WT and KO littermates (n=8). ***(D)*** Determination of percentage of fat mass of WT and KO mice using NMR imaging (n=8). ***(E)*** Determination of BMI of WT and KO mice before and after HFD feeding (n=8). ***(F)*** Representative images of Epi WAT and H&E staining of Epi from WT and KO mice after HFD

feeding. Scale bars, 50 μm. ***(G)*** Determination of Epi weights from WT and KO mice after HFD feeding and the fat pad weight normalized to body weight (n=8). ***(H)*** Representative images of SubQ WAT and H&E staining of SubQ from WT and KO mice after HFD feeding. Scale bars, 50 μm. ***(I)*** Determination of SubQ from WT and KO mice after HFD feeding and the fat pad weight normalized to body weight (n=8). ***(J)*** Representative H&E staining images of BAT and quantification of cell numbers in BAT for WT and KO mice. Scale bars, 50 μm. ***(K)*** Representative H&E staining images of livers of WT and KO mice ***(L)*** Representative Oil Red O staining images of liver for WT and KO mice. Scale bars, 50 μm. ***(M)*** Representative H&E staining images of pancreases and determination of islet size for WT and KO mice (n=8). **P < 0.01. Student's t test. Scale bars, 50 μm. *P < 0.05, **P < 0.01. All data are presented as the mean ± s.e.m.

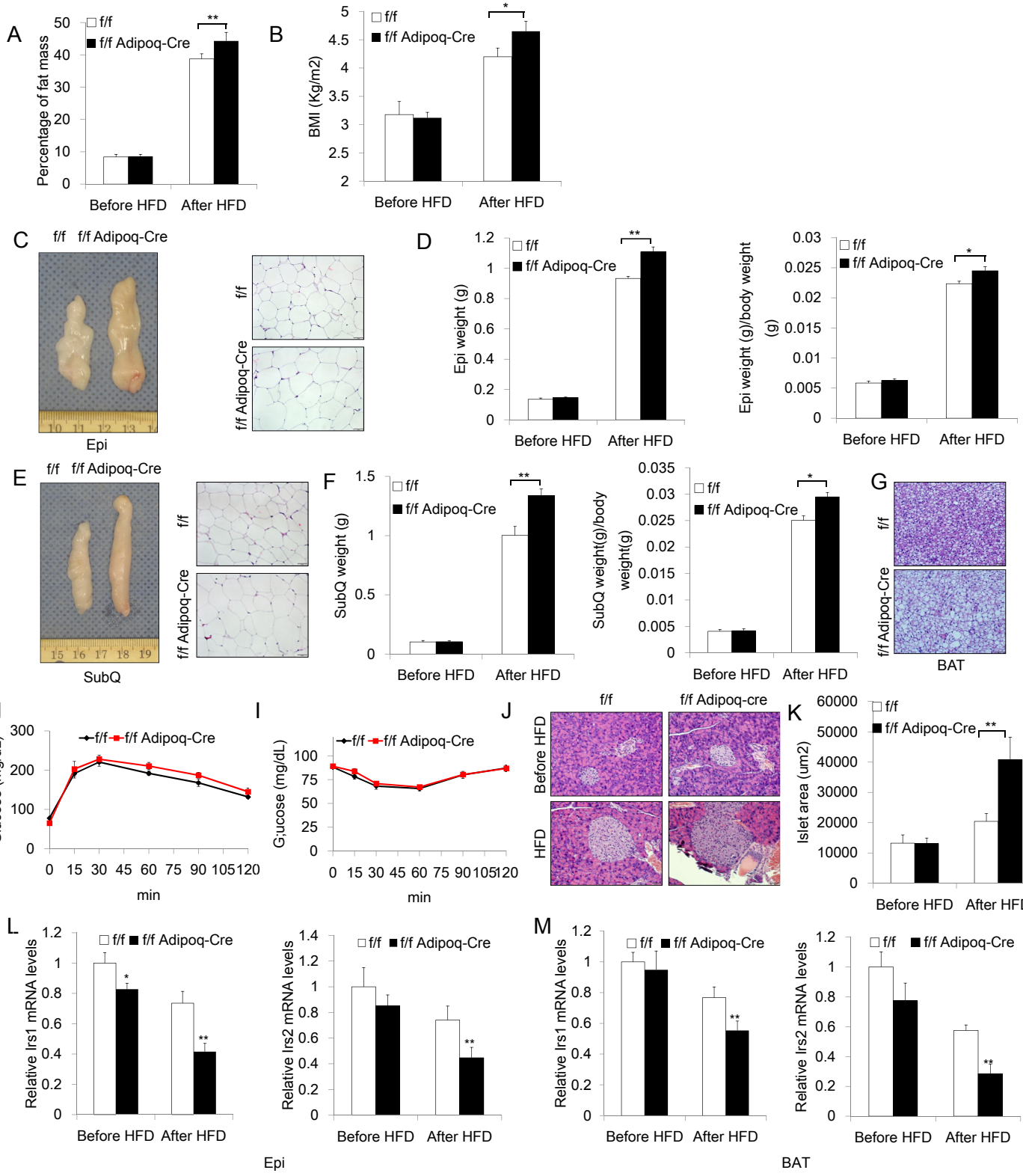

Figure. S2. ***Kdm4b$^{f/f}$Adipoq-Cre*** **mice on HFD display accelerated the onset of obesity.** ***(A)*** Determination of percentage of fat mass using nuclear magnetic resonance scanner of *Kdm4b$^{f/f}$* and *Kdm4b$^{f/f}$Adipoq-Cre* littermates upon HFD feeding for 10 weeks (n=8). ***(B)*** Determination of BMI of *Kdm4b$^{f/f}$* and *Kdm4b$^{f/f}$Adipoq-Cre* littermates upon HFD feeding for 10 weeks (n=8). ***(C)*** Representative images of Epi WAT and H&E staining of Epi from *Kdm4b$^{f/f}$* and *Kdm4b$^{f/f}$Adipoq-Cre* littermates. Scale bars, 50 μm. ***(D)*** Determination of Epi weights of *Kdm4b$^{f/f}$* and *Kdm4b$^{f/f}$Adipoq-Cre* mice and fat weight normalized to body weight before and after HFD feeding (n=8). ***(E)*** Representative images of SubQ WAT and H&E staining of SubQ from *Kdm4b$^{f/f}$* and *Kdm4b$^{f/f}$Adipoq-Cre* littermates. Scale bars, 50 μm. ***(F)*** Determination of SubQ weights of *Kdm4b$^{f/f}$*

and *Kdm4b*$^{f/f}$*Adipoq-Cre* mice and fat weight normalized to body weight before and after HFD feeding (n=8). ***(G)*** Representative H&E staining images of BAT of *Kdm4b*$^{f/f}$ and *Kdm4b*$^{f/f}$*Adipoq-Cre* mice after HFD feeding. Scale bars, 50 μm. ***(H and I)*** Plasma blood glucose during insulin tolerance test (ITT) ***(H)*** and glucose tolerance test (GTT) ***(I)*** before HFD *Kdm4b*$^{f/f}$ and *Kdm4b*$^{f/f}$ *Adipoq-Cre* mice (n=5). ***(J and K)*** Representative H&E staining images of pancreases ***(J)*** and determination of islet size ***(K)*** for *Kdm4b*$^{f/f}$ and *Kdm4b*$^{f/f}$*Adipoq-Cre* mice before and after HFD feeding (n=6). ***(L and M)*** Expression levels of markers *Irs1* and *Irs2* in WAT ***(L)*** and BAT ***(M)*** for *Kdm4b*$^{f/f}$ and *Kdm4b*$^{f/f}$ *Adipoq-Cre* mice before and after HFD feeding. (n=6). *P < 0.05, **P < 0.01. All data are presented as the mean ± s.e.m.

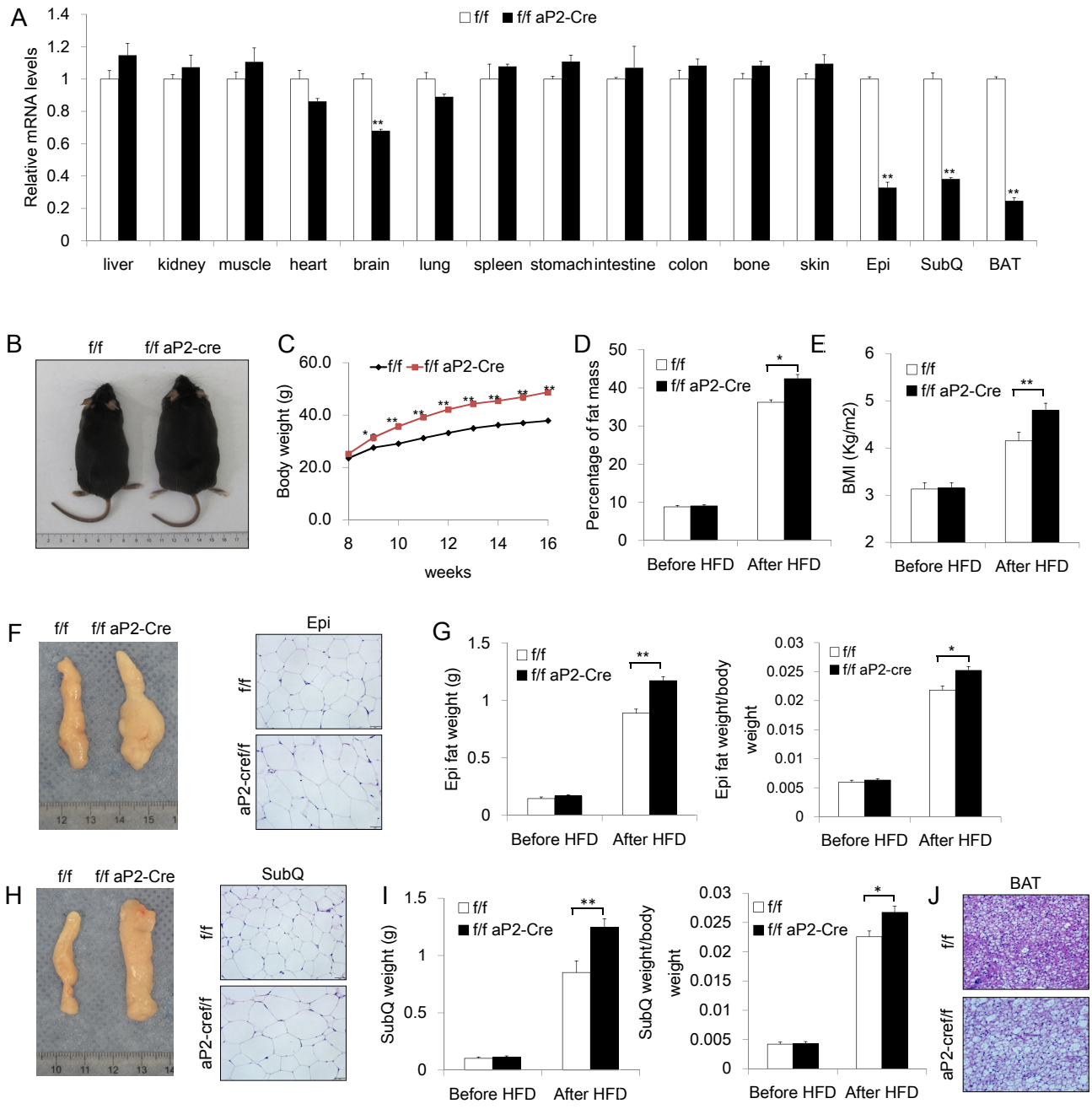

Figure. S3. ***Kdm4b$^{f/f}$ aP2-Cre*** **mice are prone to obesity following high fat diet.** ***(A)*** Verification of adipose-specific deletion of *Kdm4b* using Real Time RT-PCR (n=5). ***(B)*** Representative images of *Kdm4b$^{f/f}$* and *Kdm4b$^{f/f}$ aP2-Cre* littermates after HFD feeding. ***(C)*** Growth curve of *Kdm4b$^{f/f}$* and *Kdm4b$^{f/f}$ aP2-Cre* littermates during 8-week HFD feeding (n=8). ***(D)*** Determination of percentage of fat mass for *Kdm4b$^{f/f}$* and *Kdm4b$^{f/f}$ aP2*-Cre mice before and after HFD feeding (n=8). ***(E)*** Determination of BMI for *Kdm4b$^{f/f}$* and *Kdm4b$^{f/f}$ aP2-Cre* mice before and after HFD feeding (n=8). ***(F)*** Representative images of Epi WAT for *Kdm4b$^{f/f}$* and *Kdm4b$^{f/f}$ aP2-Cre* mice after HFD feeding and H&E staining of Epi. Scale bars, 50 μm. ***(G)*** Determination of the net weight of Epi for *Kdm4b$^{f/f}$* and *Kdm4b$^{f/f}$ aP2-Cre* mice and fat weight normalized to body weight before and after HFD feeding (n=8). ***(H)*** Representative images of SubQ WAT and H&E staining. Scale bars, 50 μm. ***(I)*** Determination of the net weight of SubQ and fat weight normalized to body weight before and after HFD feeding (n=8). ***(J)*** Representative H&E staining images of BAT for *Kdm4b$^{f/f}$* and *Kdm4b$^{f/f}$ aP2-Cre* before and after HFD feeding. Scale bars, 50 μm. *P < 0.05, **P < 0.01. All data is presented as the mean ± s.e.m.

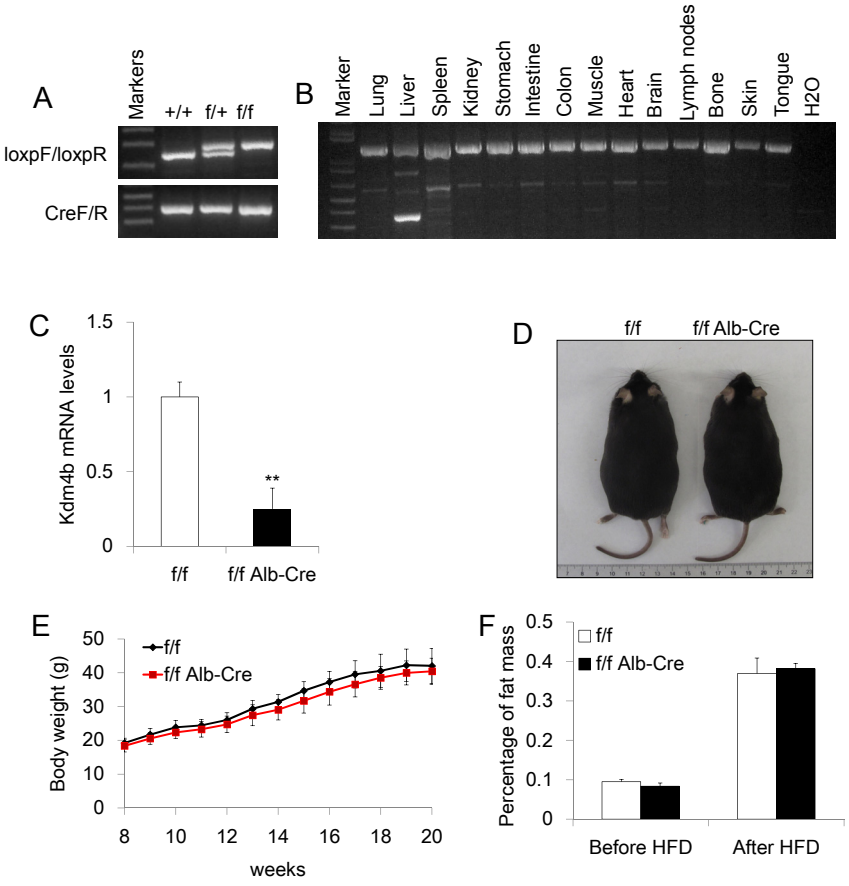

Figure. S4. ***Kdm4b*** **liver-specific knockout mice do not exacerbate diet-induced obesity.** ***(A)*** Genotyping analysis of WT, f/+ and f/f in *Kdm4b$^{f/f}$ Alb-Cre* mice. ***(B)*** DNA PCR analysis of different tissues of *Kdm4b$^{f/f}$ Alb-Cre* mice verifying liver specific deletion of *Kdm4b* gene. ***(C)*** Real-Time RT-PCR showing mRNA levels of Kdm4b in liver tissue of *Kdm4b$^{f/f}$* and *Kdm4b$^{f/f}$ Alb-Cre* mice. (n=8). ***(D)*** Representative image of *Kdm4b$^{f/f}$* and *Kdm4b$^{f/f}$ Alb-Cre* littermate after HFD feeding. ***(E)*** Growth curve of *Kdm4b$^{f/f}$* and *Kdm4b$^{f/f}$ Alb-Cre* littermates after 12 weeks of HFD (n=8). ***(F)*** Determination of percentage of fat mass by nuclear magnetic resonance scanner for *Kdm4b$^{f/f}$* and *Kdm4b$^{f/f}$ Alb-Cre* before and after HFD feeding (n=8). **P < 0.01. All data are presented as the mean ± s.e.m.

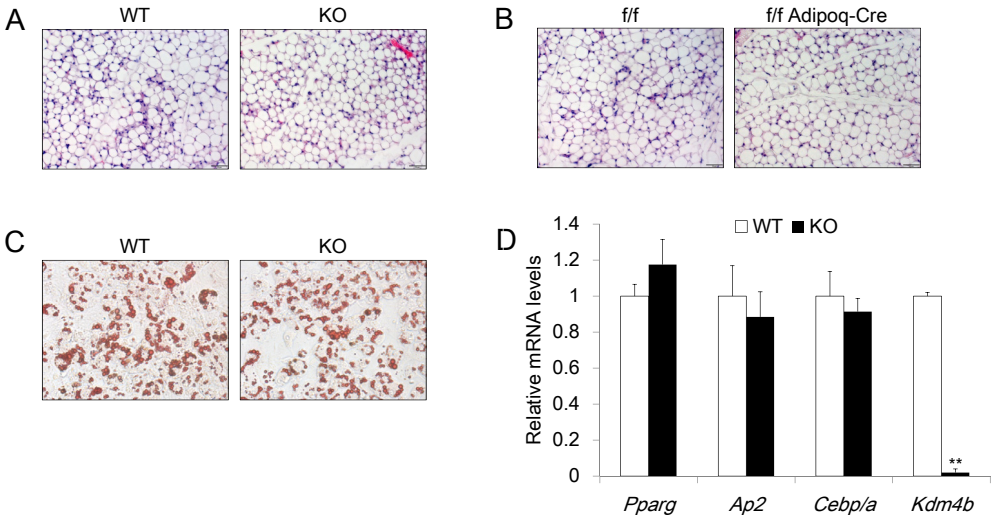

Figure. S5. KDM4B is not required for cold-induced SubQ fat browning and has no effect on adipogenic differentiation. ***(A)*** Histological examination of SubQ fat browning in WT and KO mice upon cold stimulation. ***(B)*** Histological examination of SubQ fat browning *Kdm4b*$^{f/f}$ and *Kdm4b*$^{f/f}$*Adipoq-Cre* mice upon cold stimulation. ***(C)*** Representative images of Oil Red O staining for differentiation of preadipocytes isolated from WT and KO mice. ***(D)*** Gene expression of adipogenic marker genes for preadipocytes isolated from WT and KO mice during adipogenic differentiation. Error bars represent mean ± SD for triplicate experiments. **P < 0.01.

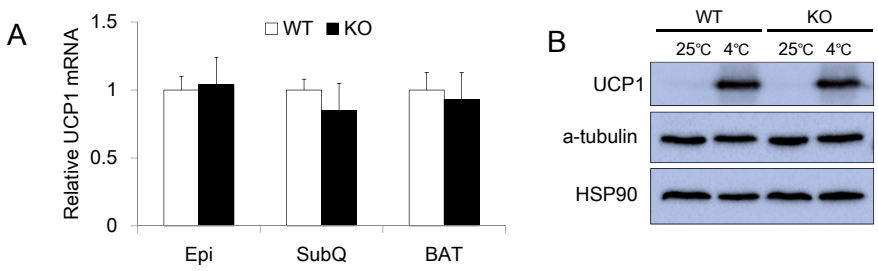

Figure. S6. The deletion of KDM4B does not impair *Ucp1* expression. ***(A)*** RT-qPCR showed the mRNA levels of *Ucp1* in Epi fat, SubQ fat and Brown fat of 2 months WT and KO mice. **P < 0.01. Data are presented as the mean ± s.e.m. ***(B)*** Western blot showed that the deletion of KDM4B did not impair cold-induced UCP1 protein expression.

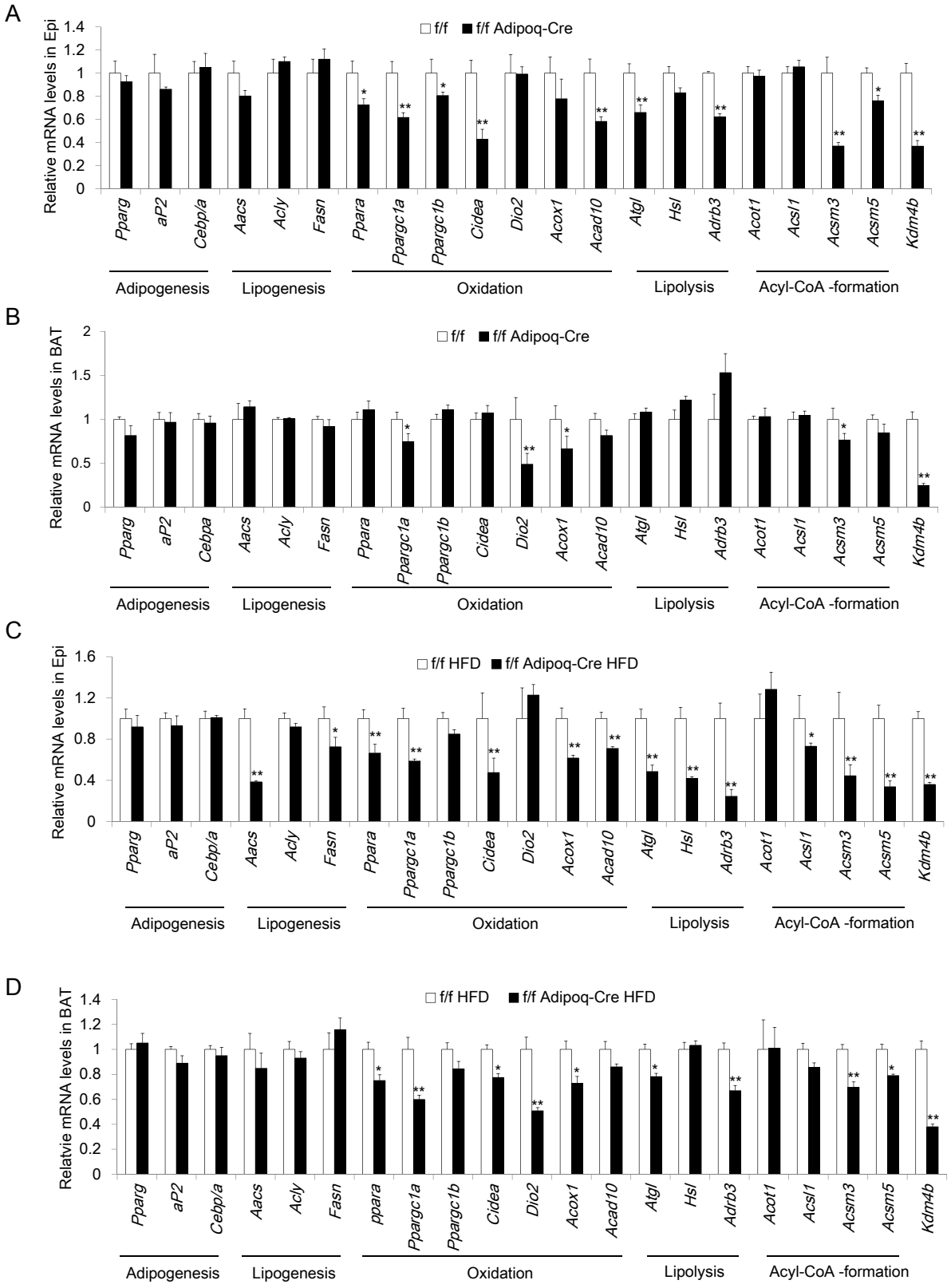

Figure. S7. KDM4B regulates metabolic genes. ***(A and B)*** Real Time RT-PCR analysis of metabolic marker genes in Epi ***(A)*** and BAT ***(B)*** of control *Kdm4b$^{f/f}$* and *Kdm4b$^{f/f}$ Adipoq-Cre mice* before HFD feeding at 2 months. ***(C and D)*** Real Time RT-PCR analysis of metabolic marker genes in Epi ***(C)*** and BAT ***(D)*** of control *Kdm4b$^{f/f}$* and *Kdm4b$^{f/f}$ Adipoq-Cre* mice after HFD feeding. *P < 0.05, **P < 0.01. Data are presented as the mean ± s.e.m.

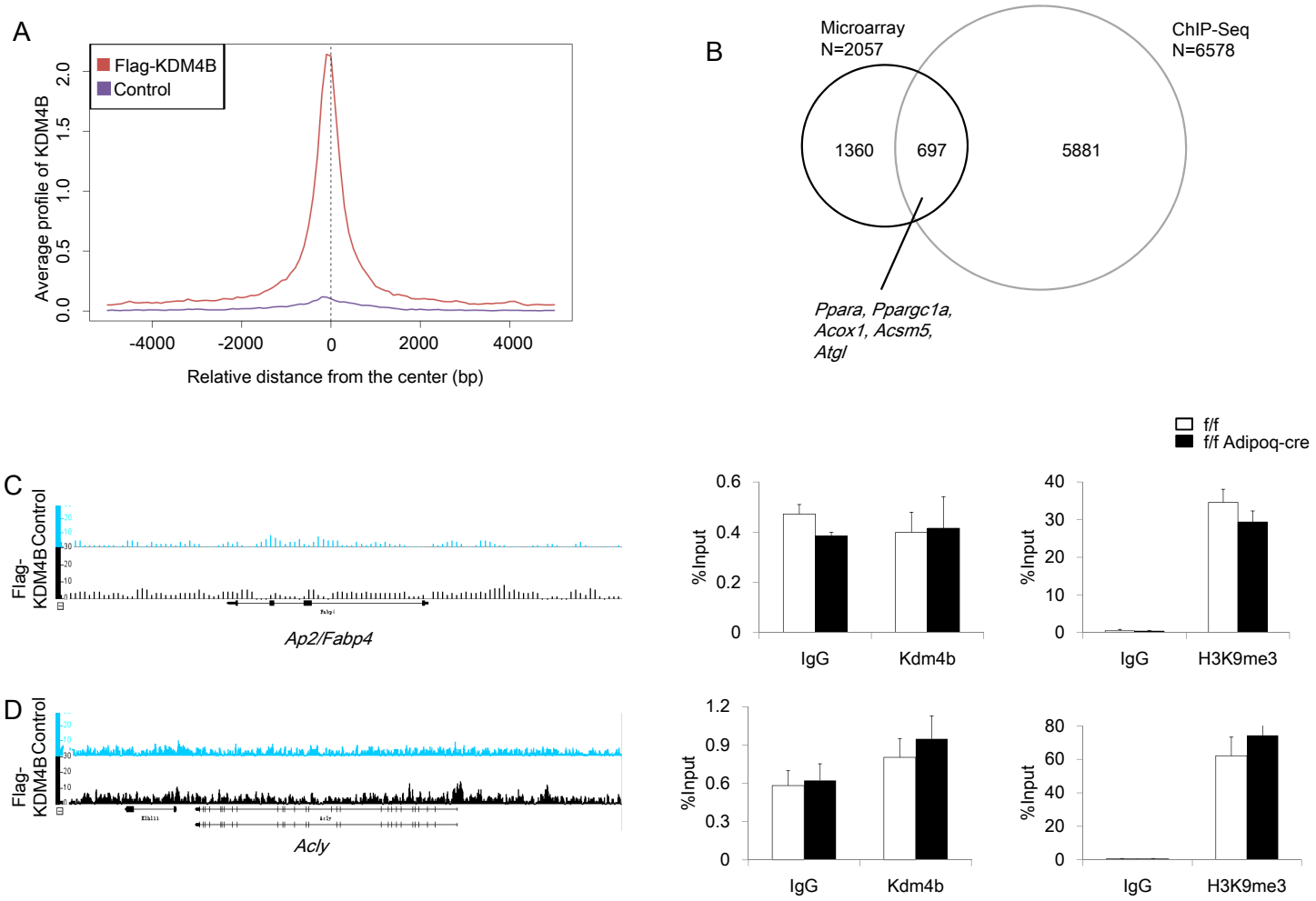

Figure. S8. H3K9me3 marks are not changed on the promoters of genes that are not regulated in *Kdm4b* KO mice. ***(A)***The average bindings of KDM4B for all refseq gene promoters, spanning ± 5 kb of the closest TSSs. Red line (Flag-KDM4B), average KDM4B binding in Kdm4b-/-/Flag-KDM4B cells with anti-Flag antibodies; Purple line (Control), average KDM4B binding in Kdm4b-/-/EV cells. ***(B)*** Venn diagram of overlap of genome-wide gene expression data and KDM4B ChIP-seq data. ***(C)*** The KDM4B occupancy and the levels of H3K9me3 marks on the promoter of *Ap2/Fabp4* were measured by ChIP-qPCR. ***(D)*** The KDM4B occupancy and the levels of H3K9me3 marks on the promoter of *Acly* were measured by ChIP-qPCR. Error bars represent mean ± SD for triplicate experiments.

Table S1. Primer list

RT-qPCR primers	Sequence 5'-3'	Size
Irs1F	CTATGCCAGCATCAGCTTCC	93bp
Irs1R	TTGCTGAGGTCATTTAGGTCTTC	
Irs2F	TCCAGGCACTGGAGCTTT	107bp
Irs2R	GGCTGGTAGCGCTTCACT	
PpargF	ATTAGATGACAGTGACTTGGC	101bp
PpargR	TGTCTTGGATGTCCTCGATG	
aP2F	GCTGGTGGTGGAATGTGTTA	89bp
aP2R	AATTTCCATCCAGGCCTCTT	
C-EBPaF	TCAGACCAGAAAGCTGAGTTGTG	100bp
C-EBPaR	TGGTCCCCGTGTCCTCCT	
AacsF	GCTGAGTTCTGGAAGTTCAG	82bp
AacsR	CATCTGCAATCCCTTTGGATG	
AclyF	TCAGTCCCAAGTCCAAGATCC	134bp
AclyR	TCTCGGGAACACACGTAGTC	
FasnF	CCAAGCAGGCACACACAATG	110bp
FasnR	AGTGTTCGTTCCTCGGAGTG	
Ppara F	AACTGGATGACAGTGACATTTCC	103bp
Ppara R	CCCTCCTGCAACTTCTCAAT	
Ppargc1aF	CCCTGCCATTGTTAAGAC	160bp
Ppargc1aR	GCTGCTGTTCCTGTTTTC	
Ppargc1bF	GAGGGCTCCGGCACTTCC	89bp
Ppargc1bR	GTACTTGCTTTTCCCAGATG	
CideaF	ACATCCAGCTCGCCCTTTTC	133bp
CideaR	CAGCGTAACCAGGCCAGTTG	
Dio2F	ATGCTGACCTCAGAAGGGCT	105bp
Dio2R	GTGCACCACACTGGAATTGG	
Acox1F	GCATCGCAGACCCTGAAGAA	144bp
Acox1R	GGTGCATCCATTTCTCCTGC	
Acad10F	CTTGGAGAAGTACCTGAAGG	106bp
Acad10R	CAGCCTGATGTAGTACGTTG	
AtglF	GCCAACGCCACTCACATCTA	90bp
AtglR	AATGTTGGCACCTGCTTCAC	
HslF	TGGAACTAAGTGGACGCAAG	91bp
HslR	TCAGACACACTCCTGCGCA	
Adrb3F	CGCTCAACAGGTTTGATGGC	95bp
Adrb3R	GTTCCAGGGGACTCACTAGC	
Acot1F	ATGATGGTTTGGAGGTTGGG	143bp
Acot1R	CCAGCCCTTGAATCAGCAC	
Acsl1F	AGCCACCATGTGACCTCTC	114bp
Acsl1R	CATCGTCGTAGTAGTACACC	
Acsm3F	ATCTACTTCACCAGTGGGAC	143bp

Acsm3R	CCTGTATCTGAAGTATTCCAC	
Acsm5F	GCTCATGATGTGTTGGATGTG	104bp
Acsm5R	CTCTTGACTTCTGTTCCTGAG	
Cox7a1F	GAGGACGCAAAATGAGGGC	91bp
Cox7a1R	GCCACACGGTTTTCTAAGTGG	
Atp5c1F	CCTTGACTTTCAACCGCACC	114bp
Atp5c1R	CCTCTTGTCTGAGGATGCAACT	
Atp5g2F	GCGGCCTCTGACTTCACTTA	54bp
Atp5g2R	GAAATGGCGCTGGTTTGGAA	
36B4F1	GCCAGCTCAGAACACTGGTCTA	60bp
36B4R1	ATGCCCAAAGCCTGGAAGA	
HprtF	TGCTGACCTGCTGGATTACA	120bp
HprtR	TTTATGTCCCCCGTTGACTGA	
Kdm4bF	TGTCTCACCCATCTATGGAG	96bp
Kdm4brealR	ATGTCTAGGATGGTCCTCAG	
ChIP Primers		
Ppargc1aChIPF3	AGGGCTCCGGTTTAGAGTTG	142bp
Ppargc1aChIPR3	TGCCTCAGTGAAGTAACGCTT	
Ppargc1a 8kbup ChIPF	ACACTGCGTTCTTGTCTTGT	110bp
Ppargc1a 8kbup ChIPR	CGAAAAACCGCACAACTGGT	
PparalphachipF2	CTGTCCGCCACTTCGAGTC	58bp
PparalphachipR2	GAACACCAATGTTCGGAGCC	
Ppara 8kbup ChIPF	CTTCTGTAGGCAGCAGCACA	54bp
Ppara 8kbup ChIPR	CAGGCAGGTCCAAGTGCTAA	
Acox1ChipF1	GACCCTTGACACCCATTCCC	107bp
Acox1ChipR1	GGACTCACCTCCTTTCAGGC	
Acox1 8kbup ChIPF	ACGGACTACTGACTACGGGA	53bp
Acox1 8kbup ChIPR	TTGGCACTGCAGGTACATGAT	
AtglChIPF	CATTGGTCTCCCCGAACTGG	71bp
AtglChIPR	GTCACAGCAGTTTGTAGCGG	
Atgl 4kupChIPF	TAGGAGGGTCCAGGGTTCTG	108bp
Atgl 4kupChIPR	GCTGGGTCAACTCCCATGAA	
Acsm5ChIPF3	CACAGTCAGCCTTCAGTGGT	112bp
Acsm5ChIPR3	TCCCTTGGGGCAAATTCCTC	
Acsm5 8kbdown ChIPF3	GGACCAATCTTGGAGCAGTCT	80bp
Acsm5 8kbdown ChIPR3	GCCAAATAACCTCCACGAGC	
aP2ChIPF1	TTGACAGTCAAAACAGGAACC	83bp
aP2ChIPR1	CTGGCAATGATCACTGGACT	
AclyChIPF	CTGCTTAGCCTGTGAGCTGAT	137bp
AclyChIPR	GTGGCTCTCTGTCCGTAAGC	

Genotyping primers		
CreF	GCATTACCGGTCGATGCAACGAGTGATGAG	408bp
CreR	GAGTGAACGAACCTGGTCGAAATCAGTGCG	
Kdm4bloxpF	ACCCAGGACTGATGTTCACA	221bp/291bp
Kdm4bloxpR	GAAAGAAGACCTGAGCTGTC	
Kdm4bGenoF	TGGCTCTCTTAGGGGCAGTC	

References

1. Folch J, Lees M, & Sloane Stanley GH (1957) A simple method for the isolation and purification of total lipides from animal tissues. The Journal of biological chemistry 226(1):497-509.
2. Chan CB, et al. (2015) Activation of muscular TrkB by its small molecular agonist 7,8-dihydroxyflavone sex-dependently regulates energy metabolism in diet-induced obese mice. Chem Biol 22(3):355-368.
3. Vergnes L, Chin R, Young SG, & Reue K (2011) Heart-type fatty acid-binding protein is essential for efficient brown adipose tissue fatty acid oxidation and cold tolerance. J Biol Chem 286(1):380-390.
4. Ye L, et al. (2012) Histone demethylases KDM4B and KDM6B promotes osteogenic differentiation of human MSCs. Cell Stem Cell 11(1):50-61.
5. Gollub J & Sherlock G (2006) Clustering microarray data. Methods Enzymol 411:194-213.
6. Li J, et al. (2013) LATS2 suppresses oncogenic Wnt signaling by disrupting beta-catenin/BCL9 interaction. Cell Rep 5(6):1650-1663.
7. Haim Y, Tarnovscki T, Bashari D, & Rudich A (2013) A chromatin immunoprecipitation (ChIP) protocol for use in whole human adipose tissue. Am J Physiol Endocrinol Metab 305(9):E1172-1177.
8. Li J, et al. (2017) KDM3 epigenetically controls tumorigenic potentials of human colorectal cancer stem cells through Wnt/beta-catenin signalling. Nature communications 8:15146.